PRIFYSGOL ABERYSTWYTH UNIVERSITY

Aberystwyth University

A comparison of multiple luminescence chronometers at Voordrag, South Africa

Colarossi, D.; Duller, G. A.T.; Roberts, H. M.; Tooth, S.; Botha, G. A.

Published in:
Quaternary Geochronology

DOI:
10.1016/j.quageo.2020.101094

Publication date:
2020

Citation for published version (APA):
Colarossi, D., Duller, G. A. T., Roberts, H. M., Tooth, S., & Botha, G. A. (2020). A comparison of multiple luminescence chronometers at Voordrag, South Africa. *Quaternary Geochronology*, *60*, [101094]. https://doi.org/10.1016/j.quageo.2020.101094

Document License
CC BY-NC-ND

General rights
Copyright and moral rights for the publications made accessible in the Aberystwyth Research Portal (the Institutional Repository) are retained by the authors and/or other copyright owners and it is a condition of accessing publications that users recognise and abide by the legal requirements associated with these rights.

• Users may download and print one copy of any publication from the Aberystwyth Research Portal for the purpose of private study or research.
• You may not further distribute the material or use it for any profit-making activity or commercial gain
• You may freely distribute the URL identifying the publication in the Aberystwyth Research Portal

Take down policy
If you believe that this document breaches copyright please contact us providing details, and we will remove access to the work immediately and investigate your claim.

tel: +44 1970 62 2400
email: is@aber.ac.uk

Download date: 04. May. 2023

A comparison of multiple luminescence chronometers at Voordrag, South Africa

D. Colarossi*[1,2], G.A.T. Duller[2], H.M. Roberts[2], S. Tooth[2], G.A. Botha[3]

[1]Department of Human Evolution, Max Planck Institute for Evolutionary Anthropology, Deutscher Platz 6, 04103 Leipzig, Germany
[2]Department of Geography and Earth Sciences, Aberystwyth University, Aberystwyth, SY23 3DB, Wales
[3]Council for Geoscience, 139 Jabu Ndlovu Street, Pietermaritzburg, South Africa

*Corresponding author: debra_colarossi@eva.mpg.de

Highlights

1. Existing radiocarbon and feldspar $IRSL_{50}$ ages for Voordrag are incorrect
2. $IRSL_{50}$ signal affected by anomalous fading
3. Single grain quartz OSL and K-feldspar post-IR IRSL ages match
4. Saturation of OSL signal identified using I_n/I_0 ratio and proportion of saturated grains
5. Paired quartz/feldspar measurements can identify effect of saturation on quartz OSL signal

Keywords:

Single grains
multiple grains
K-feldspar post-IR IRSL
quartz OSL
radiocarbon
saturation

Abstract

A suite of 10 samples collected from an 11 m thick colluvial sequence at Voordrag, KwaZulu-Natal, South Africa, have been used to undertake a comparison of different luminescence methods. Good agreement is found between single grain quartz optically stimulated luminescence (OSL) and single grain K-feldspar post-infrared infrared-stimulated luminescence (post-IR IRSL) ages, with the exception of the basal samples where the quartz OSL signal is saturated. Multiple grain quartz OSL consistently yields ages older than single grain OSL methods. Multiple grain feldspar ages derived from the $IRSL_{50}$ signal are underestimated due to anomalous fading. A previously published radiocarbon chronology yields ages that are younger than those from single grain quartz OSL and post-IR IRSL, and this is most likely due to contamination with younger carbon. Identifying the effect of saturation on the quartz OSL signal remains challenging when quartz is dated in isolation. However, using a paired quartz/feldspar dating approach is an effective way of identifying the impact of saturation on the OSL signal.

1. Introduction

Single grain luminescence dating has become increasingly common over the last two decades and is now routinely applied to both the quartz optically stimulated luminescence (OSL) signal (e.g. Porat et al. 2006, Jacobs et al. 2008, Armitage et al. 2011, Feathers and Pagonis 2015, Doerschner et al. 2016) and the K-feldspar post-infrared infrared stimulated luminescence (post-IR IRSL) signal (e.g. Reimann et al. 2012, Trauerstein et al. 2014, Rhodes 2015, Smedley et al. 2016, Carr et al. 2019). Single grain dating is a powerful tool within the array of luminescence methods because it allows identification of grains with aberrant OSL characteristics (e.g. Roberts et al. 1999, 2015, Yoshida et al. 2000, Jacobs et al. 2003, Olley et al. 2004), as well as sources of inhomogeneity, such as contamination via sediment mixing or roof spall (e.g. Arnold and Roberts 2009, Jacobs et al. 2011). Unwanted grains can be excluded prior to age calculation. These advantages make single grain dating of particular use in heterogeneously-bleached sediments, as it becomes possible to base calculations on grains that were well-bleached at deposition (e.g. Porat et al. 2006, Trauerstein et al. 2014), resulting in more accurate dating.

https://doi.org/10.1016/j.quageo.2020.101094
Available online 28 May 2020

A number of studies have compared single grain luminescence ages with radiocarbon ages to assess the reliability of the method. Good agreement between single grain quartz OSL ages and radiocarbon ages was reported by Olley et al. (2004) between 50 ka and 1.5 ka for a deep-sea marine core, by Guerrero et al. (2018) from 41.5 ± 3.9 ka to 15.1 ± 0.3 ka for palaeolake sites in Spain, and by Wood et al. (2016) between 50 ka and 30 ka at an archaeological site in Western Australia. Fewer studies have looked at single grain analyses of feldspars. Carr et al. (2019) reported single grain post-IR $IRSL_{225}$ ages in good agreement with radiocarbon ages younger than ~25 ka from two sites in the Mojave Desert, whilst Brill et al. (2018) and Riedesel et al. (2018) found good agreement between single grain post-IR IRSL ages and historical records for tsunami deposits.

Recently, however, Thomsen et al. (2016) questioned the validity of single grain measurements for ages older than 20 ka. The premise of their study came from Murray et al. (2012) who concluded that incomplete bleaching is expected to be of lesser importance for samples in this age range. In their study, Thomsen et al. (2016) found their quartz single grain OSL measurements underestimated their multiple grain measurements and radiocarbon ages by up to 40 % when "standard" rejection criteria (i.e. recycling, recuperation and test dose uncertainty) were applied. They suggested that applying two additional criteria, based on the characteristic saturation dose (D_0) and the fast ratio, could improve the agreement of their single grain ages with independent age control at the cost of reducing the accepted grain population by an order of magnitude or more, and concluded that their multiple-grain ages were more accurate.

The aim of this paper is to compare ages obtained using multiple luminescence chronometers at the multiple grain and single grain level, within the range of radiocarbon dating, for a colluvial sequence of sediments and palaeosols at Voordrag, South Africa. The site preserves an important, semi-continuous, late Quaternary terrestrial archive that was previously dated with luminescence and radiocarbon dating by Clarke et al. (2003). Their multiple grain luminescence ages were based on the infrared stimulated luminescence (IRSL) signal from large aliquots of K-feldspar measured with a single aliquot additive dose (SAAD) method utilising the dose correction method (Duller 1994). Since their original chronology was produced there have been major advances in luminescence dating. The advent of the single aliquot regenerative dose (SAR) protocol (Murray and Wintle 2003) improved the reliability of quartz OSL, the post-IR IRSL protocol (Thomsen et al. 2008) provided access to a more stable K-feldspar signal that is less influenced by anomalous fading, and technical development of the automated Risø readers (Bøtter-Jensen et al. 2000) provided the ability to measure equivalent doses (D_e) for individual grains. This paper will compare multiple grain and single grain quartz OSL, and single grain feldspar post-IR IRSL, with the previously published multiple grain IRSL, and radiocarbon results of Clarke et al. (2003).

2. Study site

The Masotcheni Formation is a succession of dominantly sandy colluvial sediments with interbedded palaeosols found widely across northern KwaZulu-Natal, South Africa. The Formation is observed at the site of Voordrag (27°44'30''S 31°19'24''E), ~52 km east of Vryheid (Figure 1a) and has previously been described by Botha et al. (1992), Botha (1996) and Clarke et al. (2003). The succession exposed at Voordrag is distinct from others in the region as it preserves several untruncated palaeosols, making it a key late Quaternary terrestrial archive for the southern African interior. Although the sedimentary succession is ~18 m thick, palaeosols are preserved only in the upper ~11 m. The succession sits on the lower transportational midslope of the northern face of Ntumbane Hill and was deposited within a bowl-shaped depression eroded into the Vryheid Formation sandstone bedrock (Botha et al. 1992). This depression had a restricted outlet during the Late Pleistocene and Holocene and received episodic inputs of sediment transported mainly by sheet wash from the surrounding slopes, implying short (< 1 km) transport distances (Figure 1b). Extensive recent incision has produced a donga (gully) with an areal extent of ~13,586 m^2 and exposed a composite stratigraphy of stacked colluvial sedimentary units with intercalated palaeosols or split palaeosol horizons (Figure 1c). The sandy colluvial sedimentary units are

suitable for luminescence dating while the organic-enriched palaeosol topsoil horizons provide materials for radiocarbon dating.

2.1. Existing chronology

During the early 1990s nine soil samples were collected from the colluvial units and dated using the IRSL signal on large aliquots of K-feldspar. The IRSL ages ranged from 99.2 ±9.1 ka to 10.8 ± 1.2 ka (Clarke et al. 2003). Eleven samples were collected from the palaeosol layers for radiocarbon dating. Measurements were undertaken on disseminated organic material within clay sub-samples, concentrated from the bulk buried surface profiles. The organic content of the clay sub-samples ranged from 0.6 to 2.9 % (Table 1). Sieving in the field was used to remove the <20 µm size fraction and provide sufficient mass of carbon for further processing. Acid solubles were also removed with the intention of increasing the concentration of organic matter for analysis (Clarke et al. 2003). The clay sub-samples were then combusted to carbon dioxide, and after purification were analysed in proportional radiation counters. The previously reported radiocarbon ages (calibrated using the IntCal98 calibration curve) have been recalibrated (Table 1) using OxCal v4.2 (Bronk Ramsey 2009) and the Southern Hemisphere calibration curve (ShCal13, Hogg et al. 2013).

3. Methods and instrumentation

3.1. Sample collection and laboratory preparation

The sedimentary succession at Voordrag represents pulses of colluvial sedimentation that resulted in net aggradation, interspersed with periods of slope stability during which pedogenesis occurred near the surface horizons of the colluvial strata. Samples for luminescence dating were collected from near the base of each colluvial layer, to provide an approximate age for the onset of deposition. In contrast, the radiocarbon sample from the overlying palaeosol should provide both a minimum age for cessation of deposition and an approximate age for the period during which pedogenesis occurred. Thus each luminescence age should be older than the overlying radiocarbon age and younger than the underlying radiocarbon age i.e. the radiocarbon ages should provide a bracketing age range for the luminescence ages (Figure 1d).

Ten samples (VRD09-VRD01, and VRD10, Figure 1d) were collected for luminescence dating by hammering tubes into colluvial sediments exposed in the donga sidewalls. Laboratory preparation under subdued red light conditions involved a 10 % v.v. dilution of concentrated (37 %) hydrochloric acid (HCl) and 20 vols hydrogen peroxide (H_2O_2) to remove carbonates and organics respectively. Samples were dry-sieved (to obtain the 180-212 µm fraction) and separated using sodium polytungstate (SPT) at densities of 2.70 g cm^{-3} and 2.62 g cm^{-3} for quartz and 2.58 g cm^{-3} and 2.53 g cm^{-3} for K-feldspar. The internal potassium (K) concentration was determined for each feldspar separate using GM-beta counting (GMBC) on a Risø GM-25-5 beta counter (Bøtter-Jensen and Mejdahl, 1988). Values ranged between 10.1 ± 0.4 % and 15.1 ± 1.1 %, implying that these samples are composed predominantly of K-rich feldspar grains (the theoretical limit for feldspars is ~14 % by weight). Quartz grains were etched in 40 % hydrofluoric acid (HF) for 45 min in order to remove the alpha-irradiated outer surface of the grains and any lingering feldspar grains. In contrast, feldspar grains were not etched in hydrofluoric acid (HF) due to concerns about anisotropic removal of the surface (Duller, 1992).

3.2. Dosimetry

External beta dose rates were measured using a low level Risø GM-25-5 beta counter. External gamma dose rates were measured directly using an Ortec DigiDart portable field gamma spectrometer equipped with a 2-inch NaI crystal, and corrected for the modern water content (measured in the laboratory) prior to dosimetry calculation. The gamma spectrometer was

calibrated using the blocks described by Rhodes and Schwenninger (2007), and monitored using a local standard in Aberystwyth immediately prior to and following fieldwork to ensure reproducibility. The 'threshold' technique (Løvborg and Kirkegaard, 1974) was used for data analysis, thus avoiding the uncertainty associated with identification of specific peaks as occurs when using the 'Windows' approach. The external alpha dose rate was measured directly through thick source alpha counting (TSAC) using Daybreak 582 and 583 alpha counters. Whilst the external alpha dose contribution can be disregarded for quartz due to the etching process, it must be included in the K-feldspar dose rate calculation because the grains were not HF etched. Following correction for the lower efficiency of alpha radiation compared to beta and gamma radiation (using an a-value of 0.11 ± 0.03, Balescu and Lamothe 1993) and grain size attenuation, the external alpha dose rate ranged from 0.09 ± 0.03 to 0.17 ± 0.05 Gy ka^{-1}, equivalent to ~3 % of the sample dose rate.

External alpha, beta and gamma dose rates for both minerals were corrected for grain size attenuation and water content using a burial water content of 30 ± 5 %. This water content is relatively high with respect to the modern measured water contents (Table 2), although it is lower than the saturation water contents (41-48 %) measured for four samples. The burial water content is based on the value of Clarke et al. (2003) who cite the presence of pollen from wetland flora, ferruginous plinthic mottling and iron-stained root channels in support of this seemingly high value. This evidence implies colluvium accretion and subsequent pedogenesis in a poorly drained environment subject to fluctuating vadose zone conditions (Botha et al. 1992). Thus, the deposits would have been wet throughout sediment accretion within the basin and the current dryness would only have affected the sub-surface moisture contents after donga formation (Clarke et al. 2003). The cosmic dose rate was calculated using the method of Prescott and Hutton (1994). Conversion factors for dosimetry calculations were taken from Guérin et al. (2011) and dose rate data are included in Table 2.

3.3. Instrumentation and equivalent dose measurements

3.3.1.Multiple grain (MG) quartz

Multiple grain (MG) luminescence measurements were undertaken on an automated Risø TL/OSL-DA-15 reader using blue diodes (470 nm, 80 mW cm^{-2}) with detection by an EMI 9635 QA photomultiplier fitted with a 7.5 mm thick Hoya-U340 filter. Laboratory irradiations were made using a calibrated $^{90}Sr/^{90}Y$ beta source, with a dose rate of 0.0912 Gy s^{-1}. Quartz MG measurements were made using the single aliquot regenerative dose (SAR) protocol (Table 3a) with the IR-OSL depletion ratio (Duller 2003) used to assess samples for feldspar contamination. Measurements were made on small (~2 mm) aliquots mounted on aluminium discs with SilkoSpray™ silicone oil. The preferred grain size for all measurements was the 180-212 µm grain size fraction, however measurements for samples Aber215/VRD06, Aber215/VRD04, Aber215/VRD02 and Aber215/VRD10 where made on the 150-180 µm fraction because insufficient material remained in the preferred size fraction following the final HF etching phase.

Data analysis was undertaken in Analyst v4.53 (Duller, 2015). Dose response curves (DRCs) were fit with a single saturating exponential (SSE) function. Equivalent dose (D_e) values were determined by integrating the initial 0.8 s of the decay curve and subtracting the signal from a late background, taken from the last 8 s of the decay curve. D_e values from individual aliquots were accepted only if: (i) the recycling ratio was within 10 % of unity; (ii) recuperation was less than 5% of the natural signal; (iii) the error on the test dose signal was less than 3 standard deviations of the background signal; and (iv) the uncertainty on the test dose luminescence measurement was less than 10%. Samples were considered to be saturated when L_n/T_n was equal to or greater than the signal from the maximum measured regeneration dose. The additional D_0 screening criteria of Thomsen et al. (2016) was applied to the quartz datasets, but failed to improve the results. Therefore, it was not included as an acceptance criterion for the final age analysis (all data are included in the supplementary information).

3.3.2.Single grain (SG) quartz

Single grain quartz stimulation used the 10 mW green laser (532 nm, Bøtter-Jensen et al. 2010) with detection by an EMI 9235 QA photomultiplier fitted with a 2.5 mm thick Hoya-U340 filter. Laboratory irradiations were made using a calibrated $^{90}Sr/^{90}Y$ beta source, with a dose rate of 0.0370 Gy s^{-1}. Quartz measurements were made on individual grains (180-212 µm, unless stated otherwise) using a similar SAR protocol (Table 3b) to that used for MG measurements. All SG measurement (i.e. preheat temperatures, IR-OSL depletion ratio, etc.) and analysis (i.e. DRC fitting, etc.) parameters were identical to the MG parameters. Decay curves showed a rapid initial decrease typical of a signal dominated by the fast component (Figure 2a). Considerable variability was observed (Figure 2a, inset) between dose response curves (DRCs) for SG quartz measurements for individual samples as reported in previous studies (e.g. Roberts et al. 1999, Jacobs et al. 2003, Duller 2012, Wood et al. 2016). Single grain quartz D_e values were determined by integrating the initial 0.1 s of the decay curve and subtracting the signal from a late background, taken from the last 0.2 s of the decay curve. Equivalent dose (D_e) values from individual grains were screened using the same criteria as the MG D_e values (Section 3.3.1).

3.3.3.Single grain (SG) K-feldspar

Stimulation of the post-IR IRSL signal from single grains of feldspar (180-212 µm, unless stated otherwise) was achieved with a focused 150 mW IR laser (830nm, Bøtter-Jensen et al. 2010), following IR stimulation at 50 °C of all of the feldspar grains mounted on SG discs simultaneously using the IR LED array (875 nm, 146 mW cm^{-2}). A post-IR $IRSL_{225}$ protocol (Table 3c) was selected, based on dose recovery and fading tests. A test dose ~30 % of the expected natural D_e was used to avoid issues related to the carry-over of charge between measurements (Yi et al. 2016, Colarossi et al. 2018). Luminescence emitted in the blue region of the spectrum was detected by an EMI 9235 QA photomultiplier filtered by a combination of 2 mm Schott BG-39 and 2 mm Corning 7-59 glass. Laboratory irradiations were made using a calibrated $^{90}Sr/^{90}Y$ beta source, with a dose rate of 0.0370 Gy s^{-1}. Dose response curves (DRCs) for K-feldspar measurements were fit with a single saturating exponential (SSE), double saturating exponential (DSE) or single exponential plus linear (SEPL) function to obtain the "best fit" based on the reduced chi squared parameter, and showed a variation in shape (Figure 2b) similar to that of the quartz DRCs. Single grain K-feldspar D_e values were calculated by integrating the initial 0.165 s of the decay curve and subtracting the last 0.33 s of the decay curve. The same acceptance criteria used in the quartz analysis (Section 3.3.1) were applied to the K-feldspar D_e data.

4. *Multiple grain (MG) quartz OSL chronology*

Two samples (Aber215/VRD06 and Aber215/VRD01) were selected for a preheat-dose recovery test (Table 4) to determine the measurement parameters for the SAR protocol (Table 3a). A set of twenty four aliquots was prepared for each sample and the natural signal removed using two blue diode stimulations at 30 °C for 100 s, separated by a 10 ks pause to allow the 110 °C trap to empty (Wintle and Murray 2006). A subset of three aliquots was used for each preheat temperature between 160 °C and 300 °C at 20 °C intervals. Each aliquot was irradiated with a known beta dose similar to the expected natural dose for the relevant sample. For the two samples, the SAR procedure was able to recover the given dose for preheats from 160 to 280°C. Therefore, a regeneration dose preheat temperature of 220 °C for 10 s was selected for all further measurements, in combination with a test dose preheat of 160 °C for 10 s.

To determine the natural D_e for the samples, up to 24 single aliquots of each sample were measured. The single aliquot natural dose distributions for all of the samples except Aber215/VRD09 have low overdispersion (OD) values ranging between 8 % and 26 % (Table 5), and normally distributed dose distributions. Therefore, the Central Age Model was used for these

samples. The uppermost sample (Aber215/VRD09) has an OD of 75 % and a well-defined leading edge to the distribution, typical of a heterogeneously bleached sample, and so the unlogged Minimum Age Model (MAM_{UL}, Arnold et al. 2009) with a sigma-b value of 0.15 Gy was used for this sample.

The MG OSL ages, ranging from 0.64±0.06 to 69.0±6.9 ka (Table 5 and Figure 3a, yellow squares), are generally stratigraphically consistent and show an overall increase with depth. There is one age inversion at Aber215/VRD04 and the ages for the two lowest samples (Aber215/VRD01 and Aber215/VRD10) are younger than Aber215/VRD02 that overlies them, although all three ages are within uncertainty of one other. The proportion of aliquots whose natural OSL signal is at saturation (n_{sat}) increases with depth (Figure 3b) from 0 % (Aber215/VRD09) to 86 % (Aber215/VRD10), but the impact of this saturation upon the reliability of the OSL age is difficult to define. Wintle and Murray (2006) suggested a maximum reliability threshold of $2D_0$ for dating with the quartz OSL signal (i.e. $D_e < 2D_0$), where D_0 is the characteristic saturation dose of the dose response curve. More recently, Chapot et al. (2012) observed a divergence between natural and laboratory DRCs for Chinese loess at ~150 Gy and cautioned that D_e estimates above this value should be considered as potential underestimations. In this study at Voordrag, the lowest six samples (from Aber215/VRD05 downwards) are beyond the value of $2D_0$ recommended by Wintle and Murray (2006), and the lowest three samples (from Aber215/VRD02 downwards) are beyond the D_e value of 150 Gy recommended by Chapot et al. (2012), and thus need additional investigation.

5. *Single grain (SG) quartz OSL chronology*

5.1. Dose recovery tests

The SAR protocol used for SG quartz OSL (Table 3b) used the same parameters as the MG measurements (Table 3a, Section 4). Additional dose recovery tests were completed on single grains of quartz to ensure the selected SAR protocol was appropriate for SG measurements. Three samples were selected based on their stratigraphic location: i) an upper sample (Aber215/VRD09), ii) a middle sample (Aber215/VRD06), and iii) a lower sample (Aber215/VRD01). For each sample, 5 single grain discs were prepared and the same dose recovery experiment used on multiple grains (Section 4) was undertaken. The upper and middle samples were able to successfully recover known beta doses of 5 and 90 Gy (dose recovery ratios of 1.02 ± 0.01 and 0.91 ± 0.03) respectively and OD values were <11 % (Table 3). In contrast, the lower sample failed to recover a known dose of 150 Gy (ratio 0.79 ± 0.04) and also has a much higher OD of 57 % (Table 4). As was seen with the natural MG data, the proportion of saturated grains increases with dose (Table 4).

5.2. Single grain equivalent dose (D_e) distributions

The single grain dose distributions for the natural D_e (Figure 4a-c) have relatively low overdispersion (OD) values, ranging from 12-36 % (Table 5) combined with normal distributions. The exception to this is the distribution for the uppermost sample (Aber215/VRD09, Figure 4a) which has an OD of 110 % and is positively skewed with a well-defined leading edge, indicative of the effect of heterogeneous bleaching. The unlogged Minimum Age Model (MAM_{UL}) of Arnold et al. (2009) was used for Aber215/VRD09 with a sigma_b value of 0.20 Gy based on the OD observed in the dose recovery tests (Table 4). For all other samples the Central Age Model (CAM) of Galbraith et al. (1999) was applied.

The two lowermost samples, Aber215/VRD01 and Aber215/VRD10, (OD 12 % and 34 %, respectively) have a very limited number of D_e values in their distribution (n = 5, Table 4) since the majority of measured grains that passed the acceptance criteria for these sample are in saturation (for a detailed list of grain failures see Table 6).

5.3. Single grain quartz OSL ages

The SG OSL ages, ranging from 0.32 ± 0.03 to 57.2 ± 11.5 ka (Figure 3a and Table 5), are generally stratigraphically consistent and show an overall increase with depth. One notable age inversion occurs within the sequence, with the age of Aber215/VRD04 being older than the underlying age of Aber215/VRD03. There are no obvious differences in the luminescence

characteristics to explain the aberrant behaviour of Aber215/VRD04. A grain size from 150-180 µm was used for analysis of this sample, and this may have resulted in more than one grain occupying a single hole on the disc, but given that heterogeneous bleaching does not appear to be a problem for these samples, this is unlikely to be the cause of this result.

6. Single grain K-feldspar post-IR $IRSL_{225}$ chronology

6.1. Dose recovery tests

Dose recovery tests were undertaken on the same three samples (Aber215/VRD09, Aber215/VRD06 and Aber215/VRD01) used for the single grain quartz dose recovery tests. Three single grain discs were prepared for each sample and bleached in the Honlë SOL-2 solar simulator for 48 hours. The discs were then irradiated with a known beta dose (Table 4), and measured using the post-IR $IRSL_{225}$ protocol outlined in Table 3c. All three samples successfully recovered a given dose (ratios of 1.02 ± 0.01, 0.99 ± 0.01 and 0.94 ± 0.01 respectively), OD values were below 15 %, and saturation of the post-IR IRSL signal was not observed in any of the samples (Table 4).

An additional dose recovery test was undertaken on sample Aber215/VRD09 to assess the residual signal remaining in the grains after bleaching. Two single grain discs were prepared and bleached in the solar simulator for 48 hours, however in this instance no beta dose was administered (i.e. a given dose of 0 Gy). The dose distribution (n =146, n_{sat} = 0) had an OD of 62 % and a mean D_e of 0.36 ± 0.03 Gy (Figure 5). Sohbati et al. (2012) reported a similarly low residual value of 0.93 ± 0.80 Gy for laboratory-bleached samples measured with the post-IR $IRSL_{225}$ protocol.

6.2. Fading measurements

The same three samples used for the dose recovery tests were used to test for the presence of anomalous fading. Three small (~2 mm) aliquots for each sample were prepared and bleached in the Honlë SOL-2 solar simulator for 48 hours to remove the stored signal. Following this step, the aliquots were irradiated with a beta dose similar to the expected average D_e (5 Gy, Aber215/VRD09; 100 Gy, Aber215/VRD06; 301 Gy, Aber215/VRD01), preheated immediately following irradiation as per Auclair et al. (2003), and stored for varying periods of time before measurement. The delay between irradiation and measurement ranged from 10 min to 42 days and yielded a mean g-value of 1.53 ± 0.22 %/decade for the post-IR $IRSL_{225}$ signal. Two recent studies have reported fading rates measured from quartz (1.3 ± 0.3 %/decade, Thiel et al. 2011 and 1-2%/decade, Lowick and Valla 2018) which is thought not to suffer from anomalous fading. It has been suggested that low g-values like these may be a laboratory artefact, and so following Thiel et al. (2011), fading corrections were not applied to the post-IR $IRSL_{225}$ D_e values for the samples from Voordrag.

6.3. Single grain equivalent dose distributions

The K-feldspar single grain D_e distributions (Figure 4d-f) display a higher degree of scatter than the quartz distributions for the same samples (compare Figure 4a-c). Overdispersion (OD) values are variable, ranging from 28 % to 101 % (Table 5). Reimann et al (2012) and Smedley et al (2012) suggested that microdosimetry due to variations in internal K content of individual feldspar grains may contribute to the OD observed for feldspars, but this is unlikely in this study given the high measured K contents (10-15%, Section 3.1) which are close to the limit for feldspars. The uppermost sample (Aber215/VRD09) of the sedimentary succession has the highest percentage OD (101 %), with a positively skewed distribution and a well-defined leading edge apparent in the radial plot (see Figure 4d), indicative of heterogeneous bleaching. This was also seen in the quartz dose distribution for this sample. The dose distributions for samples from Aber215/VRD08 to Aber215/VRD02 (see Figure 4e) are normally distributed. The lowermost samples Aber215/VRD01 (see Figure 4f) and VRD10 display what appears to be a normal distribution, but one that is very broad with a ~725 Gy spread in the D_e values. It is worth noting that the maximum range in K-feldspar D_e values for sample Aber215/VRD09

is 165 Gy, which is ~100 Gy greater than that of the paired quartz dose distribution for this sample (i.e. 61 Gy, compare Figure 4a, d).

The broad distributions prove somewhat difficult to interpret for age calculations. Based on the high overdispersion (OD) and the strongly skewed dose distribution, the unlogged-MAM of Arnold et al. (2009) was used on the uppermost sample (Aber215/VRD09). A sigma_b value of 0.20 Gy was selected based on the OD observed in the dose recovery tests (Table 4). For the remainder of the samples, based on the relatively lower percentage OD, and the more normal distributions, the CAM of Galbraith et al. (1999) was used to calculate the ages.

6.4. Single grain post-IR $IRSL_{225}$ ages

The single grain K-feldspar chronology, ranging from 0.43 ± 0.03 to 109 ± 4 ka, generally increases with depth, with the exception of one age inversion at the bottom of the sequence (Figure 6a, red triangles and Table 5). Sample Aber215/VRD01 slightly overestimates with respect to the underlying Aber215/VRD10, but we are unable to see any difference in the luminescence characteristics that could explain this.

There is no evidence of saturation of the post-IR $IRSL_{225}$ signal in any of the K-feldspar samples. The proportion of saturated grains remains near zero (n_{sat} < 3 %) throughout the sedimentary succession (Figure 6b and Table 5) and all D_e values are well below the suggested $2D_0$ threshold level. The D_0 for the Voordrag samples is ~350 Gy, which is comparable to the range of published D_0 values for single grain post-IR $IRSL_{225}$ measurements (e.g. 40-200 Gy, Rhodes 2015; ~306 Gy, Carr et al. (2019); ~435 Gy, Colarossi et al. 2018; ~240-325 Gy, Smedley et al. 2016).

7. Discussion

7.1. Comparison of multiple grain (MG) and single grain (SG) quartz ages

The ages obtained using the multiple grain (0.64±0.06 to 69.0±6.9 ka) and single grain (0.32 ± 0.03 to 57.2 ± 11.5 ka) quartz data sets are broadly similar (Figure 3). Analysis of the D_e distributions from both data sets show that the Voordrag samples are well-bleached, with the exception of the uppermost sample (Aber215/VRD09). Although both chronologies are generally stratigraphically consistent, the MG ages are consistently older than the SG ages by a factor of 1.2-2.0, with the exception of the two lowermost samples that overlap within uncertainty. The single grain data can be transformed to create synthetic small aliquots (each containing 100 grains) by summing the OSL signal from all the grains on each single grain disc. The resulting synthetic aliquot D_e values (calculated using the "sum-all grains" feature in Analyst, Duller 2015) show an improved match with the MG measurements (with a ratio of 0.8-1.2). Thus, the difference between MG and SG D_e values is likely the result of excluding saturated grains and grains with aberrant OSL characteristics from the single grain data sets.

Both MG and SG quartz OSL chronologies, although stratigraphically consistent, appear to reach a maximum age of ~60 ka (Figure 3a). This may be a reflection of rapid accumulation at the base of the section, or the effect of saturation of the quartz OSL signal on the ages. Thus, the ages reported for the lowest two samples (Aber215/VRD01 and Aber215/VRD10) may be minimum ages for both the MG and SG chronologies.

7.2. Saturation of the OSL signal and its impact on the quartz ages

Saturation of the OSL signal should be observable within the succession, based on the failure of sample Aber215/VRD01 to recover a known dose (see Section 5.1). However, given the overall increase in ages with depth, it is not immediately obvious where in the succession saturation of the quartz OSL signal occurs. The most commonly used approach to assess the extent of saturation is the $2D_0$ criterion (Wintle and Murray 2006). Applying the $2D_0$ maximum reliability threshold to the SG OSL data, shows all samples have $D_e < 2D_0$ (D_0 ranging from 33 ± 2 Gy to 63 ± 2 Gy, Table 5) except for the two lowermost samples (Aber215/VRD01 and Aber215/VRD10). Similarly, applying the ~150 Gy D_e threshold value of Chapot et al. (2012) shows the two lowermost samples, with D_e values of 137 ± 20 Gy and 195 ± 38 Gy respectively,

should be treated as potential underestimates. Failure of these two threshold value tests supports the hypothesis that the two lowermost samples are in saturation.

Another relatively simple assessment of the extent of saturation is calculating the proportion of saturated grains present within the accepted dose distribution. A large proportion of saturated grains within the dose distribution would unfairly bias the distribution towards lower D_e values, thereby underestimating the luminescence age (e.g. Thomsen et al. 2016, Trauerstein et al. 2014). In these samples, the proportion of saturated grains increases with depth (Figure 3b) from 4 % (Aber215/VRD09) to 92 % (Aber215/VRD01). Furthermore, more than half of the grains in the dose distributions of the four lowermost samples are in saturation (n_{sat} > 59 %), which brings into question the validity of these four ages and not only the lowest two ages (based on $2D_0$ and D_e > 150 Gy).

The comparison of the natural light level of the burial dose ($L_n/T_n = I_n$) with the maximum light level (I_0) when the data are fit by a single saturating exponential (SSE) function (Fig. 3c) is another way to attempt to quantify the extent of saturation (e.g. Lowick and Valla 2018). A SSE is defined by the equation $I = I_0 \left(1 - e^{-D/D_0}\right)$, where I is the sensitivity corrected OSL signal (L_x/T_x) resulting from dose D (Gy), D_0 is the characteristic saturation dose and I_0 the maximum OSL signal intensity of the saturating component. The I_n/I_0 ratio increases very rapidly in both datasets (Figure 3c). For the SG OSL data, the uppermost sample (Aber215/VRD09) has a value of ~20 %, but the sample directly below it in the succession (Aber215/VRD08) is ~73 %. Below this, the I_n/I_0 ratio increases steadily up to ~114 %. In contrast, the MG OSL data shows every sample > 85 % except for the uppermost sample.

It is worth noting that the point at which ~50% of grains are saturated is also the point at which the average I_n/I_0 ratio is ~85%, which equates to $2D_0$ for a single saturating exponential. This occurs somewhere between samples Aber215/VRD04 and Aber215/VRD03. However, this point does not correspond to the 150 Gy D_e threshold value, which is related to D_0 (and is thus sample dependent). Therefore, based on the Voordrag samples, it seems that the absolute threshold value (i.e. 150 Gy) is potentially more variable between sites, whilst the n_{sat} > 50 % and I_n/I_0 > 85 % (which is essentially the same as $2D_0$ for a single saturating exponential) is a more general observation that could be useful in a broader context.

It is clear that the lowest two samples (Aber215/VRD01 and Aber215/VRD10) are beyond the range of quartz OSL based on their D_0 values (i.e. $D_e > 2D_0$), the very low proportion of grains producing a finite D_e (n), the large proportion of saturated grains (n_{sat}) in the dose distribution and the ratio of the natural light level to the maximum light level (I_n/I_0 >100 %). However, based on the observed relationship between n_{sat} and the I_n/I_0 ratio, all SG quartz OSL ages down section from and including Aber215/VRD04, and all MG quartz OSL ages from Aber215/VRD03, are potentially affected by saturation. This could also explain the very large discrepancy between the MG and SG ages for Aber215/VRD02, similar to that observed in the ages for Aber215/VRD04. It is possible that the age inversion identified in the SG OSL ages at Aber215/VRD04 (and that we could not explain in Section 5.3) is a reflection of the unreliability of ages near to the level of saturation. Irrespective of this, using quartz OSL to date the lower portion of this sedimentary succession will provide a minimum burial age for some sediments due to saturation of the OSL signal.

However, it may be possible to provide clarity regarding the discrepancy between the MG and SG ages, and to assess the extent of saturation on the quartz OSL ages by using a different luminescence chronometer, specifically the post-IR $IRSL_{225}$ signal from K-feldspar.

7.3. Comparison of single grain OSL and post-IR IRSL chronologies

The K-feldspar dose distributions are much broader than the paired quartz distributions, but the agreement between the SG quartz and K-feldspar ages is good (Figure 7). Based on the extent of saturation identified in the SG OSL ages (Section 7.2) all ages below Aber215/VRD04 are

potentially minimum ages, which should underestimate with respect to the K-feldspar ages. And yet, the majority of the SG quartz and K-feldspar ages agree within 10 % of unity, with only 3 ages falling outside of this range (i.e. Aber215/VRD04, Aber215/VRD01 and Aber215/VRD10) rather than the five ages expected. This, together with the fact that the quartz OSL ages appear to increase consistently even after the signal becomes saturated (Figure 6), highlights the difficulty of working with the quartz OSL signal in the relatively high dose region where the signal is near to saturation.

The discrepancy between the SG ages for the uppermost sample Aber215/VRD09 is due to the different bleaching rates of the two minerals (e.g. Buylaert et al. 2012, Colarossi et al. 2015), with the more rapidly bleaching quartz OSL signal resulting in a younger age. Nevertheless, these samples are within two standard deviations of one another. The agreement between the SG ages for the two minerals is encouraging (given the difference in the bleaching rate between the two luminescence signals) and highlights the value of using a paired quartz/feldspar luminescence dating approach.

7.4. Comparison of single grain luminescence and radiocarbon chronologies

Both the SG quartz OSL and SG K-feldspar post-IR $IRSL_{225}$ ages are consistently older (~7,000 years) than the underlying radiocarbon ages in the upper section of the stratigraphy i.e. from the surface down to Aber215/VRD05 (Figure 6a). In contrast, there is a much smaller difference (<1,000 years) between the luminescence ages and the radiocarbon ages in the lower section of the stratigraphy, i.e. Aber215/VRD04, Aber215/VRD03 and Aber215/VRD02 are within uncertainty of their respective underlying radiocarbon ages (Figure 6a); the exception being the OSL age for Aber215/VRD04. The poorest comparison is observed in the ages from the two lowermost samples (Aber215/VRD01 and Aber215/VRD10). The radiocarbon age directly overlying Aber215/VRD01 (42.0 ± 2.9 ka) is near the limit of radiocarbon dating and so the underlying luminescence samples are beyond the dating limit of the radiocarbon technique. Furthermore, the quartz OSL ages for these two samples are minimum ages due to saturation of the OSL signal (Section 7.2). Thus, the post-IR $IRSL_{225}$ ages for these two samples are the most reliable as the signal is not influenced by saturation (Section 6.4) or anomalous fading (Section 6.2).

The discrepancy between the SG luminescence ages and the radiocarbon ages is hard to explain. As described in Section 3.1, the two chronological methods are dating different events, but they should be in stratigraphic order. A possible explanation is contamination of the radiocarbon samples with younger carbon during burial or during the wet sieving in the field. The very low carbon contents (Table 1), and the lack of any macrofossils for dating, make such contamination plausible. Radiocarbon dating of finely disseminated organic matter associated with the clay fraction of a palaeosol is difficult due to the inability to trace original organic inputs into the system, differential decomposition rates that result in the relative concentration of young carbon, and translocation of mobile organic compounds in the soil solutions (Botha et al. 1994).

The IRSL chronology published by Clarke et al. (2003) showed good agreement with the radiocarbon ages, but if these radiocarbon ages are too young due to contamination, this implies that some, or all of the ages from Clarke et al. (2003) measured with the $IRSL_{50}$ signal are also underestimated. This is explored in the next section.

7.5. K-feldspar IRSL ages measured at a low (50°C) stimulation temperature

The $IRSL_{50}$ signal used by Clarke et al. (2003) is prone to anomalous fading (Spooner, 1994; Thomsen et al., 2008; Wintle, 1973). If fading occurs but no correction is made, then ages will be underestimated.

Clarke et al. (2003) used a single aliquot additive dose procedure with a dose-correction approach (Duller 1994) which is no longer used, whilst this study used a single aliquot regenerative dose (SAR) procedure. In spite of this difference in measurement protocol, $IRSL_{50}$ ages measured by Clarke et al. (2003) and the $IRSL_{50}$ ages calculated from the first step

stimulation of the post-IR $IRSL_{225}$ protocol (steps 3 and 7 in Table 3c) in this study show good agreement (Figure 8, inset).

The approach to making fading measurements has changed significantly over the last three decades and different approaches were used by Clarke et al. (2003) and in our study. Fading measurements in Clarke et al. (2003) were made by irradiating aliquots with a known dose, and then stimulating the sample for 0.1 s using IRSL after repeated storage intervals of one month. Using this approach, no significant fading was detected for a total storage time of one year and thus no correction was applied for fading. In contrast, in this study fading measurements made following the protocol of Auclair et al. (2003) (see Section 6.2) gave a mean g-value for the first IR stimulation at 50 °C of 3.79 ± 0.20 %/decade, which implies significant fading of the $IRSL_{50}$ signal. This measurement of laboratory fading is consistent with the observation that without applying any correction, the $IRSL_{50}$ ages are younger than the post-IR $IRSL_{225}$ ages (Figure 8, open symbols). When the $IRSL_{50}$ ages are corrected for fading (Figure 8, red symbols), the ages show much better agreement with the post-IR $IRSL_{225}$ ages (and the SG OSL ages). We conclude that the $IRSL_{50}$ ages of Clarke et al. (2003) were underestimated because anomalous fading of the signal used for dating was not identified.

8. Conclusion

This paper explored multiple chronometers using the terrestrial archive preserved at Voordrag in KwaZulu-Natal, South Africa. A previous chronology for the site had shown agreement between radiocarbon and luminescence ages based on an $IRSL_{50}$ signal, but our data suggest that both chronologies were incorrect. The $IRSL_{50}$ signal from feldspar at this site suffers from anomalous fading of 3.79 ± 0.20 %/decade, but no correction was applied by Clarke et al (2003), and thus the ages are too young. We hypothesise that at least some of the radiocarbon ages are also underestimated as a result of contamination with younger carbon during burial or wet-sieving of the samples in the field.

The quartz OSL signal does not suffer from anomalous fading, and the single grain OSL data provide an excellent chronology for the upper part of the section, but the saturation of this luminescence signal becomes an increasing problem towards the base of the section. Feldspars provide a greater age range, and the post-IR $IRSL_{225}$ signal shows negligible fading. For the uppermost samples the agreement between single grain quartz OSL and single grain K-feldspar post-IR $IRSL_{225}$ ages was very good, but at depth agreement becomes more variable and less predictable.

We recommend using a paired quartz/feldspar dating approach, where suitable material is available, as an effective way of identifying the effect of saturation on the OSL signal. However, if a paired dating approach is not feasible, a relatively simple assessment of the effect of saturation can be made using the proportion of "saturated" grains which do not provide a finite D_e (n_{sat}) in conjunction with the ratio of the natural light level of the burial dose to the maximum light level (I_n/I_0) when the data are fit by a single saturating exponential function. For these samples, the point where more than 50 % of the accepted dose distribution do not provide finite D_e values (i.e. n_{sat} > 50 %) corresponds with I_n/I_0 > 85% (which corresponds mathematically to $2D_0$ for a SSE fit). An additional advantage of using I_n/I_0 rather than $2D_0$ is that I_n/I_0 can also be calculated for a double saturating exponential fit. Using an absolute threshold value (e.g. ~150 Gy, Chapot et al. 2012) is less informative due to the variation of D_0 between samples.

The new chronology for Voordrag is based on the paired quartz/feldspar SG chronology. The potential uncertainty surrounding the identification of saturation of the quartz OSL signal highlights the value of paired luminescence chronologies, particularly as single grain OSL dating of high dose samples is routinely pursued at important archaeological sites.

Acknowledgements

This research was conducted while DC was in receipt of a Doctoral Career Development Scholarship funded by Aberystwyth University. Luminescence work was supported by an NERC grant (CC003) to GATD and HMR. ST was supported by a grant from the Aberystwyth University Research Fund and

GAB by Council for Geoscience and in part through a research grant by the National Research Foundation of South Africa (Grant 109069). DC's doctoral research into luminescence dating of South African environments was supported by the Geological Society of South Africa (GSSA) Research, Education and Investment Fund, the Quaternary Research Association (QRA) New Research Workers' Award, the British Society for Geomorphology (BSG) Postgraduate Research Grant and the Department of Geology and Earth Sciences (DGES) Postgraduate Discretionary Fund. The authors would like to thank two anonymous reviewers for their comments which helped improve this manuscript.

References

Arnold, L. J., Roberts, R. G. (2009). Stochastic modelling of multi-grain equivalent dose (De) distributions: Implications for OSL dating of sediment mixtures. *Quaternary Geochronology*, 4, 204-230.

Arnold, L. J., Roberts, R. G., Galbraith, R. F., DeLong, S. B. (2009). A revised burial dose estimation procedure for optical dating of young and modern-age sediments. *Quaternary Geochronology*, 4, 306-325.

Armitage, S.J., Jasim, S.A., Marks, A.E., Parker, A.G., Usik, V.I., Uerpmann, H.-P. (2011). The Southern Route 'Out of Africa': Evidence for Early Expansion of Modern Humans into Arabia. *Science*, 331, 453-456.

Auclair, M., Lamothe, M., Huot, S. (2003). Measurement of anomalous fading for feldspar IRSL using SAR. *Radiation Measurements*, 2003, 37, 487-492.

Balescu, S., Lamothe, M. (1993). Thermoluminescence dating of the Holsteinian marine formation of Herzeele, northern France. *Journal of Quaternary Science*, 8, 117-124.

Botha, G. A. (1996). The geology and palaeopedology of Late Quaternary colluvial sediments in northern KwaZulu/Natal. Memoir 83 of the Geological Survey of South Africa. Council for Geoscience.

Botha, G., Scott, L., Vogel, J., von Brunn, V. (1992). Palaeosols and palaeoenvironments during the Late Pleistocene Hypothermal in northern Natal. *South African Journal of Science*, 88, 508-512.

Botha, G.A., Wintle, A.G., Vogel, J.C. (1994). Episodic late quaternary palaeogulley erosion in northern KwaZulu-Natal, South Africa. *Catena*, 23, 327-340.

Brill, D., Reimann, T., Wallinga, J., May, S. M., Engel, M., Riedesel, S., Brückner, H. (2018). Testing the accuracy of feldspar single grains to date late Holocene cyclone and tsunami deposits. *Quaternary Geochronology*, 48, 91 – 103.

Bronk Ramsey, C. (2009). Bayesian analysis of radiocarbon dates. Radiocarbon, 51, 337-360.

Bøtter-Jensen, L., Bulur, E., Duller, G.A.T, Murray, A.S. (2000). Advances in luminescence instrument systems. *Radiation Measurements*, 32, 523-528.

Bøtter-Jensen, L., Mejdahl, V. (1988). Assessment of beta dose-rate using a GM multicounter system. International Journal of Radiation Applications and Instrumentation Part D: Nuclear Tracks and *Radiation Measurements*, 14, 187-191.

Bøtter-Jensen, L., Thomsen, K. J., Jain, M. (2010). Review of optically stimulated luminescence (OSL) instrumental developments for retrospective dosimetry. *Radiation Measurements*, 45, 253–257.

Buylaert, J.P., Jain, M., Murray, A. S., Thomsen, K. J., Thiel, C., Sohbati, R. (2012). A robust feldspar luminescence dating method for Middle and Late Pleistocene sediments. *Boreas*, 41, 435-451.

Carr, A. S., Hay, A. S., Powell, M., Livingstone, I. (2019). Testing post-IR IRSL luminescence dating methods in the southwest Mojave Desert, California, USA. *Quaternary Geochronology*, 49, 85-91.

Chapot, M. S., Roberts, H. M., Duller, G. A. T., Lai, Z. P. (2012). A comparison of natural- and laboratory-generated dose response curves for quartz optically stimulated luminescence signals from Chinese Loess. *Radiation Measurements*, 47, 1045-1052.

Clarke, M. L., Vogel, J. C., Botha, G. A., Wintle, A. G. (2003). Late Quaternary hillslope evolution recorded in eastern South African colluvial badlands. *Palaeogeography, Palaeoclimatology, Palaeoecology*, 197, 199–212.

Colarossi, D., Duller, G. A. T., Roberts, H. M. (2018) Exploring the behaviour of luminescence signals from feldspars: implications for the single aliquot regenerative dose protocol. *Radiation Measurements*, 109, 35-44.

Colarossi, D., Duller, G. A. T., Roberts, H. M., Tooth, S., Lyons, R. (2015). Comparison of paired quartz OSL and feldspar post-IR IRSL dose distributions in poorly bleached fluvial sediments from South Africa. *Quaternary Geochronology*, 30, Part B, 233–238.

Doerschner, N., Fitzsimmons, K. E., Ditchfield, P., McLaren, S. J., Steele, T. E., Zielhofer, C., McPherron, S. P., Bouzouggar, A., Hublin, J.-J. (2016). A New Chronology for Rhafas, Northeast Morocco, Spanning the North African Middle Stone Age through to the Neolithic. *PLOS ONE*, 11, 1-34.

Duller, G.A.T. (1992). Luminescence Chronology of Raised Marine Terraces, South-West North Island, New Zealand. Unpublished thesis, University of Wales, Aberystwyth.

Duller, G.A.T. (1994). Luminescence dating of sediments using single aliquots: New procedures. *Quaternary Science Reviews*, 13, 149-156.

Duller, G.A.T. (2003). Distinguishing quartz and feldspar in single grain luminescence measurements. *Radiation Measurements*, 37, 161-165.

Duller, G.A.T. (2012) Improving the accuracy and precision of equivalent doses determined using the optically stimulated luminescence signal from single grains of quartz. *Radiation Measurements*, 47, 770-777.

Duller, G.A.T. (2015). The Analyst software package for luminescence data: overview and recent improvements. *Ancient TL*, 33, 35–42.

Feathers, J. K., Pagonis, V. (2015). Dating quartz near saturation - Simulations and application at archaeological sites in South Africa and South Carolina. *Quaternary Geochronology*, 30, Part B, 416-421.

Galbraith, R. F., Roberts, R. G., Laslett, G. M., Yoshida, H., Olley, J. M. (1999). Optical dating of single and multiple grains of quartz from Jinmium rock shelter, northern Australia: Part I, experimental design and statistical models. *Archaeometry*, 41, 339-364.

Guérin, G., Mercier, N., Adamiec, G. (2011). Dose-rate conversion factors: update. *Ancient TL*, 29, 5–8.

Guerrero, J., Gutiérrez, F., García-Ruiz, J. M., Carbonel, D., Lucha, P., Arnold, L. J. (2018) Landslide-dam paleolakes in the Central Pyrenees, Upper Gállego River Valley, NE Spain: timing and relationship with deglaciation. *Landslides*, 15, 1975-1989.

Hogg, A., Hua, Q., Blackwell, P., Niu, M., Buck, C., Guilderson, T., Heaton, T., Palmer, J., Reimer, P., Reimer, R., Turney, C., Zimmerman, S. (2013). SHCal13 Southern Hemisphere Calibration, 0–50,000 years cal BP, *Radiocarbon*, 55, 1889-1903.

Huntley, D. J., Baril, M. (1997). The K content of the K-feldspars being measured in optical dating or in thermoluminescence dating. *Ancient TL*, 15, 11–13.

Huntley, D.J., Lamothe, M. (2001). Ubiquity of anomalous fading in K-feldspars and the measurement and correction for it in optical dating. *Canadian Journal of Earth Sciences*, 38, 1093-1106.

Jacobs, Z., Duller, G.A.T., Wintle, A.G. (2003). Optical dating of dune sand from Blombos Cave, South Africa: II – single grain data. *Journal of Human Evolution*, 44, 613-625.

Jacobs, Z., Meyer, M., Roberts, R., Aldeias, V., Dibble, H., Hajraoui, M. E. (2011). Single-grain OSL dating at La Grotte des Contrebandiers ('Smugglers' Cave'), Morocco: improved age constraints for the Middle Paleolithic levels. *Journal of Archaeological Science*, 38, 3631 – 3643.

Jacobs, Z., Wintle, A.G., Roberts, R.G., Duller, G.A.T. (2008). Equivalent dose distributions from single grains of quartz at Sibudu, South Africa: context, causes and consequences for optical dating of archaeological deposits. *Journal of Archaeological Science*, 35, 1808-1820.

Lowick, S.E, Valla, P.G. (2018). Characterising the luminescence behaviour of 'infinitely old' quartz samples from Switzerland. *Quaternary Geochronology*, 43, 1-11.

Løvborg, L., Kirkegaard, P. (1974). Response of 3'X3' NaI(Ti) detectors to terrestrial gamma-radiation. *Nuclear Instruments & Methods*, 121, 239-251.

Mejdahl, V. (1987). Internal radioactivity in quartz and feldspar grains. Ancient TL, 5, 10-17.

Murray, A. S., Thomsen, K. J., Masuda, N., Buylaert, J. P., Jain, M. (2012). Identifying well-bleached quartz using the different bleaching rates of quartz and feldspar luminescence signals. *Radiation Measurements*, 47, 688-695.

Murray, A.S., Wintle, A.G. (2003). The single aliquot regenerative dose protocol: potential for improvements in reliability. *Radiation Measurements*, 37, 377-381.

Olley, J.M., De Deckker, P., Roberts, R.G., Fifield, L., Yoshida, H., Hancock, G.J. (2004). Optical dating of deep-sea sediments using single grains of quartz: a comparison with radiocarbon. *Sedimentary Geology*, 169, 175-189.

Porat, N., Rosen, S. A., Boaretto, E., Avni, Y. (2006). Dating the Ramat Saharonim Late Neolithic desert cult site. *Journal of Archaeological Science*, 33, 1341 – 1355.

Prescott, J. R., Hutton, J. T. (1994). Cosmic ray contributions to dose rates for luminescence and ESR dating: Large depths and long-term time variations. *Radiation Measurements*, 23, 497-500.

Riedesel, S., Brill, D., Roberts, H. M., Duller, G. A., Garrett, E., Zander, A. M., King, G. E., Tamura, T., Burow, C., Cunningham, A., Seeliger, M., Batist, M. D., Heyvaert, V. M., Fujiwara, O., Brückner, H. (2018). Single-grain feldspar luminescence chronology of historical extreme wave event deposits recorded in a coastal lowland, Pacific coast of central Japan. *Quaternary Geochronology*, 45, 37 – 49.

Reimann, T., Thomsen, K. J., Jain, M., Murray, A. S., Frechen, M. (2012). Single-grain dating of young sediments using the pIRIR signal from feldspar. *Quaternary Geochronology*, 11, 28-41.

Rhodes, E. J. (2015). Dating sediments using potassium feldspar single-grain IRSL: Initial methodological considerations. *Quaternary International*, 362, 14-22.

Rhodes, E.J., Schwenninger, J.-L. (2007). Dose rate and radioisotope concentrations in the concrete calibration blocks at Oxford. *Ancient TL*, 25, 5-8.

Roberts, R.G., Galbraith, R.F., Olley, J.M., Yoshida, H., Laslett, G.M. (1999). Optical dating of single and multiple grains of quartz from Jinmium rock shelter, northern Australia: Part II, results and implications. *Archaeometry*, 41, 365-395.

Roberts, R.G., Jacobs, Z., Li, B., Jankowski, N.R., Cunningham, A.C., Rosenfeld, A.B. (2015). Optical dating in archaeology: thirty years in retrospect and grand challenges for the future. *Journal of Archaeological Science*, 56, 41-60.

Smedley, R.K., Duller, G.A.T., Pearce, N.J.G., Roberts, H.M. (2012). Determining the K-content of single-grains of feldspar for luminescence dating. *Radiation Measurements*, 47, 790-796.

Smedley, R.K., Glasser, N., Duller, G.A.T. (2016). Luminescence dating of glacial advances at Lago Buenos Aires (~46 °S), Patagonia. *Quaternary Science Reviews*, 134, 59-73.

Sohbati, R., Murray, A.S., Buylaert, J.-P., Ortuño, M., Cunha, P.P., Masana, E. (2012). Luminescence dating of Pleistocene alluvial sediments affected by the Alhama de Murcia fault (eastern Betics, Spain) - a comparison between OSL, IRSL and post-IR IRSL ages. *Boreas*, 41, 250-262.

Spooner, N.A. (1994). The anomalous fading of infrared-stimulated luminescence from feldspars. *Radiation Measurements*, 23, 625-632.

Thiel, C., Buylaert, J.-P., Murray, A., Terhorst, B., Hofer, I., Tsukamoto, S., Frechen, M. (2011). Luminescence dating of the Stratzing loess profile (Austria) - Testing the potential of an elevated temperature post-IR IRSL protocol. *Quaternary International*, 234, 23-31.

Thomsen, K. J., Murray, A. S., Buylaert, J. P., Jain, M., Hansen, J. H., Aubry, T. (2016). Testing single-grain quartz OSL methods using sediment samples with independent age control from the Bordes-Fitte rockshelter (Roches d'Abilly site, Central France). *Quaternary Geochronology*, 31, 77-96.

Thomsen, K. J., Murray, A. S., Jain, M., Bøtter-Jensen, L. (2008). Laboratory fading rates of various luminescence signals from feldspar-rich sediment extracts. *Radiation Measurements*, 43, 1474-1486

Trauerstein, M., Lowick, S. E., Preusser, F., Schlunegger, F. (2014). Small aliquot and single grain IRSL and post-IR IRSL dating of fluvial and alluvial sediments from the Pativilca valley, Peru. *Quaternary Geochronology*, 22, 163-174.

Wintle, A. G. (1973). Anomalous Fading of Thermo-luminescence in Mineral Samples. *Nature*, 245, 143-144.

Wintle, A. G., Murray, A. S. (2006). A review of quartz optically stimulated luminescence characteristics and their relevance in single aliquot regeneration dating protocols. *Radiation Measurements*, 41, 369 – 391.

Wood, R., Jacobs, Z., Vannieuwenhuyse, D., Balme, J., O'Connor, S., Whitau, R. (2016). Towards an Accurate and Precise Chronology for the Colonization of Australia: The Example of Riwi, Kimberley, Western Australia. *PLOS ONE*, 11, 1-25.

Yi, S., Buylaert, J.-P., Murray, A. S., Lu, H., Thiel, C., Zeng, L. (2016). A detailed post-IR IRSL dating study of the Niuyangzigou loess site in northeastern China. *Boreas*, 45, 644-657.

Yoshida, H., Roberts, R. G., Olley, J. M., Laslett, G. M., Galbraith, R. F. (2000). Extending the age range of optical dating using single 'supergrains' of quartz. *Radiation Measurements*, 32, 439-446.

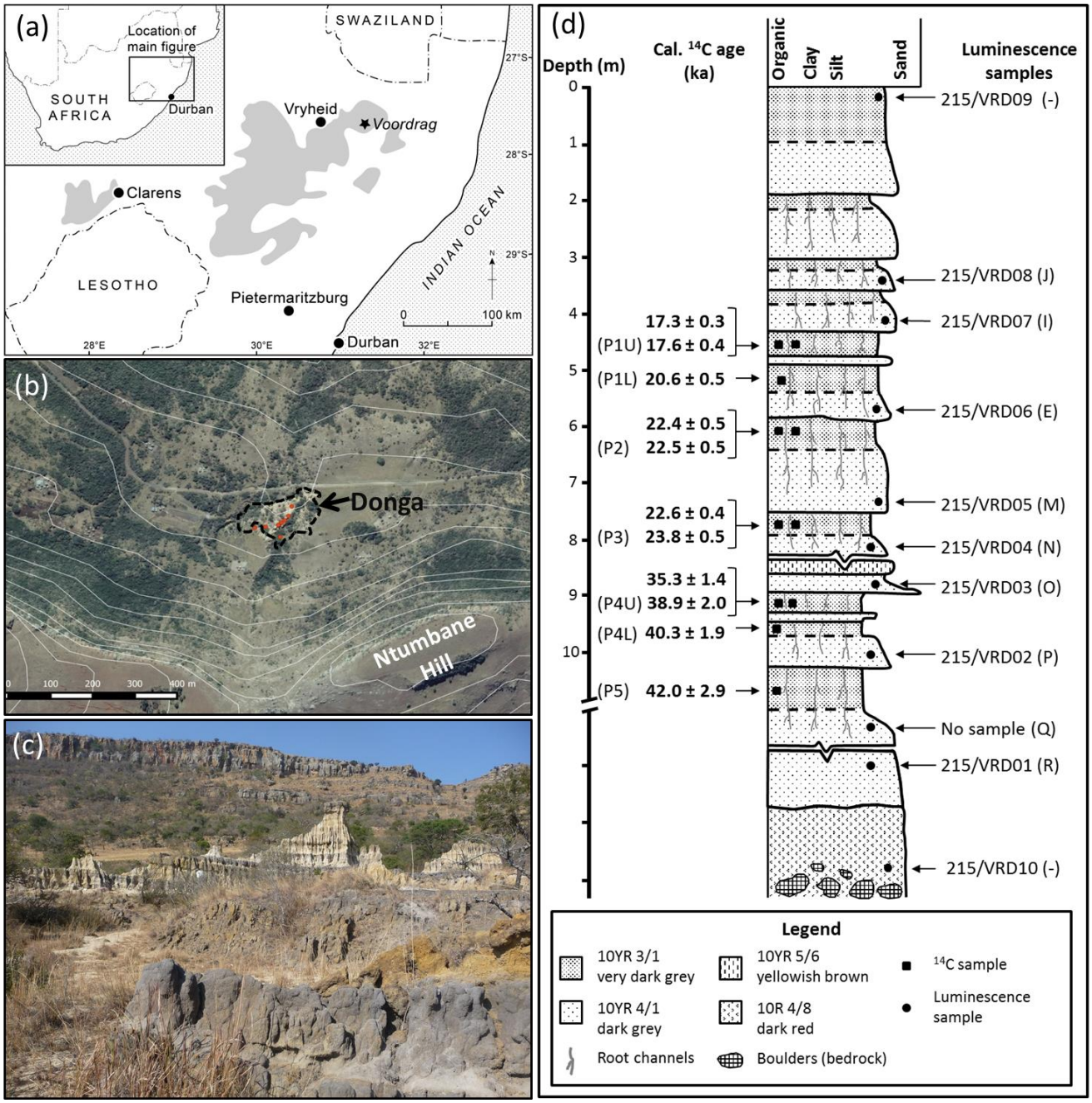

Figure 1: (a) Location of the Voordrag donga site in KwaZulu-Natal (redrawn from Botha et al. 1992). The shaded zones represent areas where the colluvial sediments of the Masotcheni Formation are widespread. (b) Location of the Voordrag donga at the foot of the Ntumbane Hill highlighting the very short transport distance (source: South Africa Department of Rural Development and Land Reform, National Geospatial Information). (c) Photograph of the central donga wall showing the interbedded colluvial sedimentary units and palaeosols. (d) Composite stratigraphy (adapted from Clarke et al. 2003) with the recalibrated radiocarbon ages of Clarke et al. (2003) collected from palaeosols, and location of the ten luminescence samples (VRD09 to VRD01, and VRD10) collected from colluvial sediments for this study. The sample IDs for the Clarke et al. (2003) $IRSL_{50}$ ages are included in brackets (J to R). There are no corresponding samples for Aber215/VRD09, Aber215/VRD10 and Q, respectively.

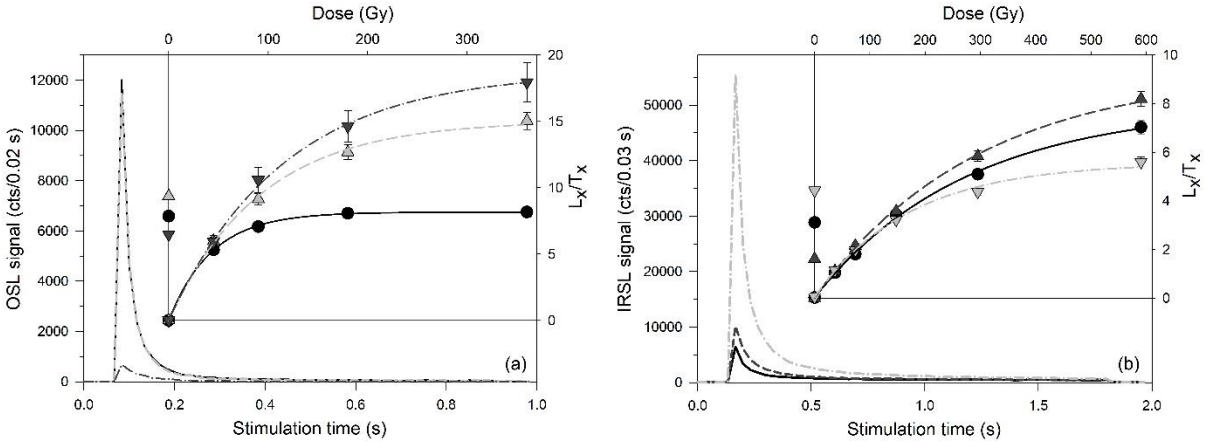

Figure 2: Dose response curves for individual (a) quartz and (b) K-feldspar grains from sample Aber215/VRD06, and the corresponding natural signals.

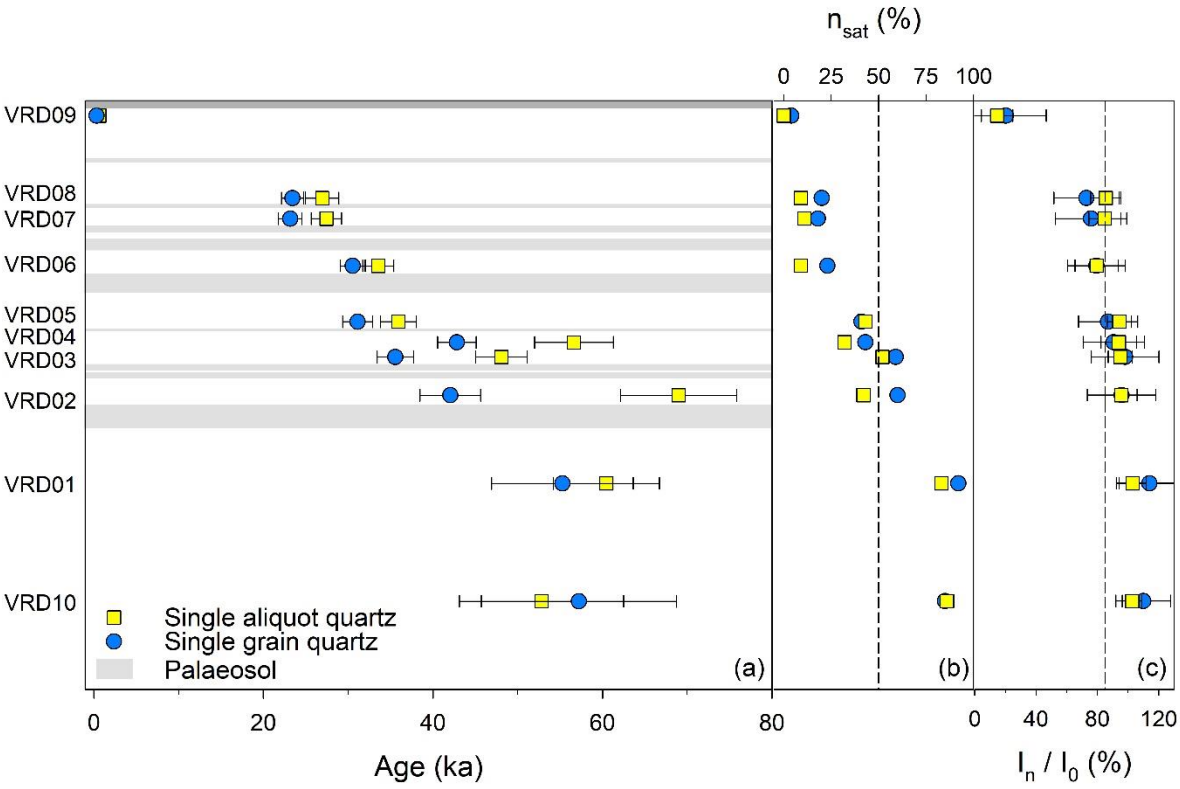

Figure 3: a) Comparison of the multiple grain (MG, yellow squares) and the single grain (SG, blue circles) quartz OSL chronologies. Sample codes are listed on the far-left and are prefixed by Aber215/ e.g. Aber215/VRD09. The relative depth of the composite section is ~15 m. b) The proportion of saturated aliquots/grains (n_{sat}) in the accepted dose population. c) The ratio of the natural light level of the burial dose ($L_n/T_n = I_n$) with the maximum light level (I_0) when the data are fit by a single saturating exponential (SSE) function. Data shown are the mean ± standard deviation of the ratios for each individual aliquot/grain included in the dose distribution (n) and saturated grain (n_{sat}) distribution.

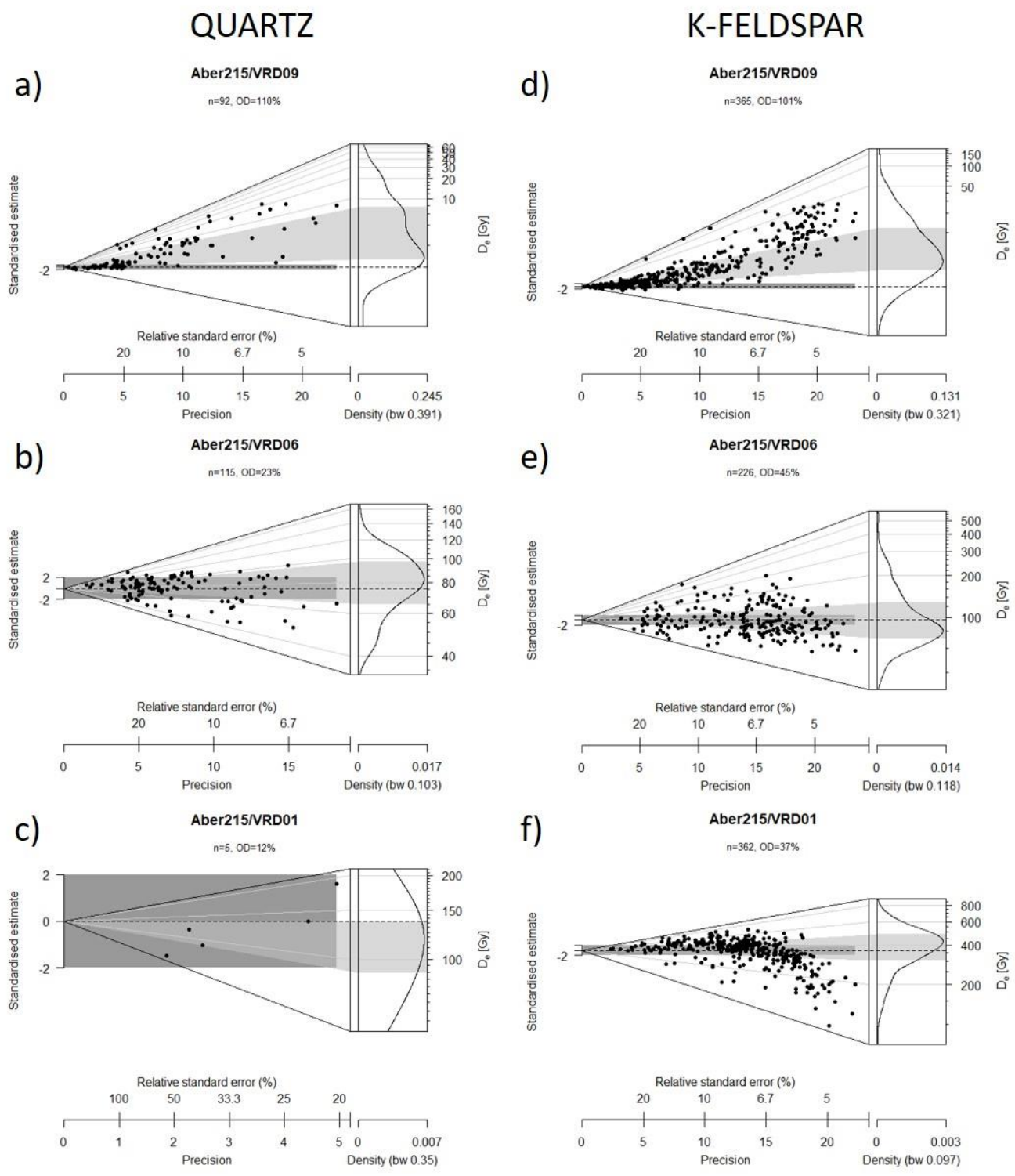

Figure 4: Abanico plots of single grain quartz (a, b, c) and K-feldspar (d, e, f) dose distributions for samples from the top (Aber215/VRD09), middle (Aber215/VRD06) and bottom (Aber215/VRD01) of the composite sedimentary section; the dark grey bar denotes the 2σ region about the MAM D_e value for sample Aber215/VRD09 and the CAM D_e value for samples Aber215/VRD06 and Aber215/VRD01.

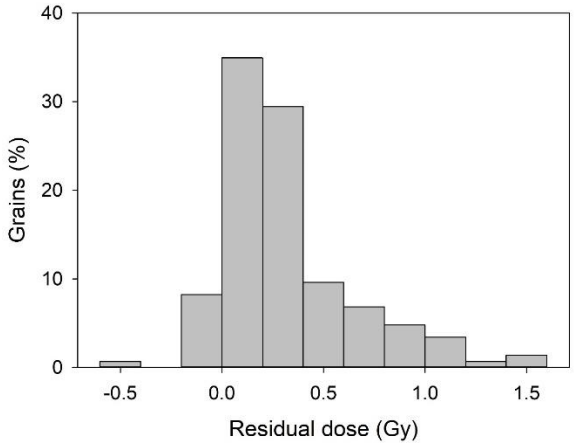

Figure 5: Histogram showing the distribution of residual doses measured for individual grains of K-feldspar using the post-IR $IRSL_{225}$ signal.

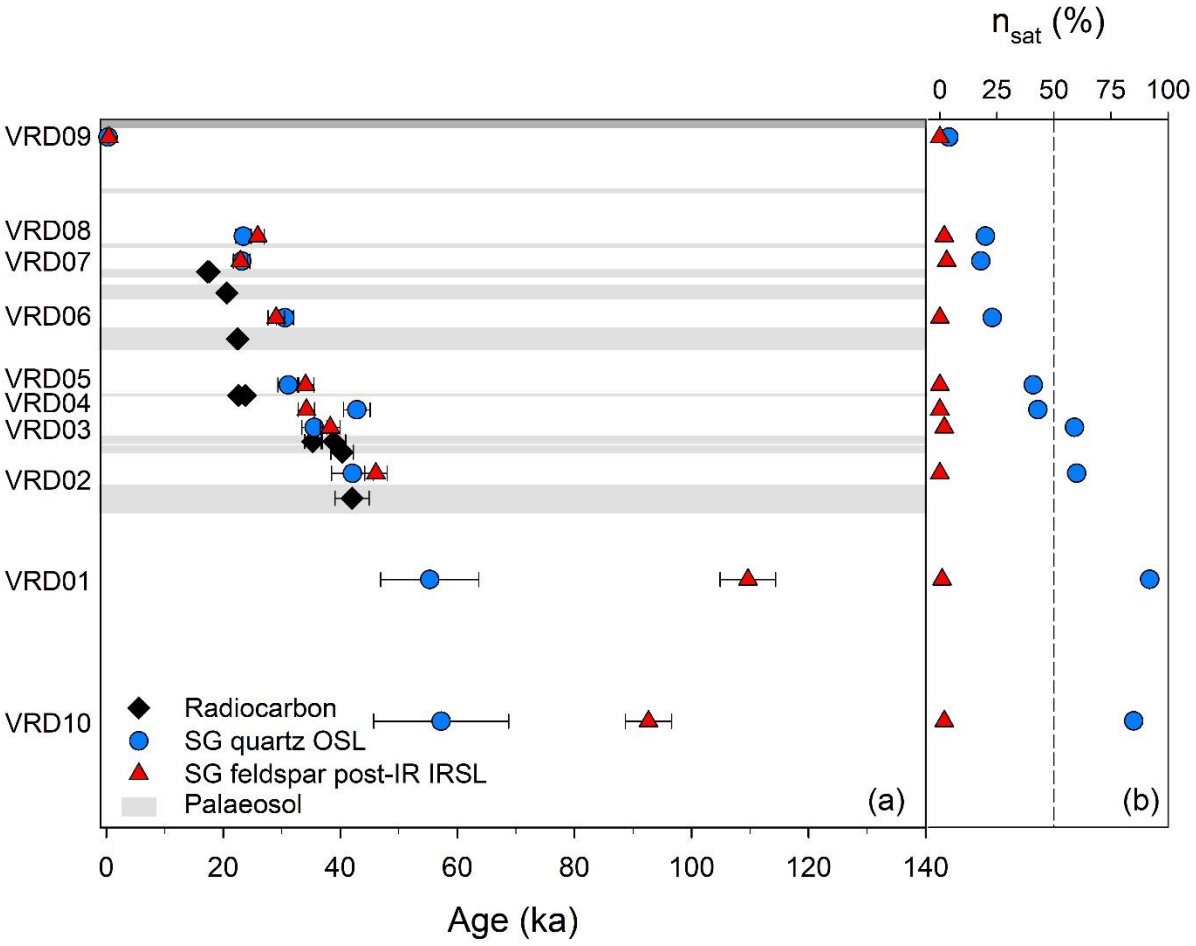

Figure 6: a) Single grain ages from quartz OSL (blue circles) and feldspar post-IR $IRSL_{225}$ (red triangles) from colluvial sediments. Radiocarbon ages (black diamonds) are shown for comparison and the location of the palaeosol layers in the section are indicated by the grey bars. Sample IDs are included in the left margin and have the prefix Aber215/ (e.g. Aber215/VRD09). The relative depth of the composite section is ~15 m. b) The proportion of saturated grains (n_{sat}) that passed the acceptance criteria for each sample.

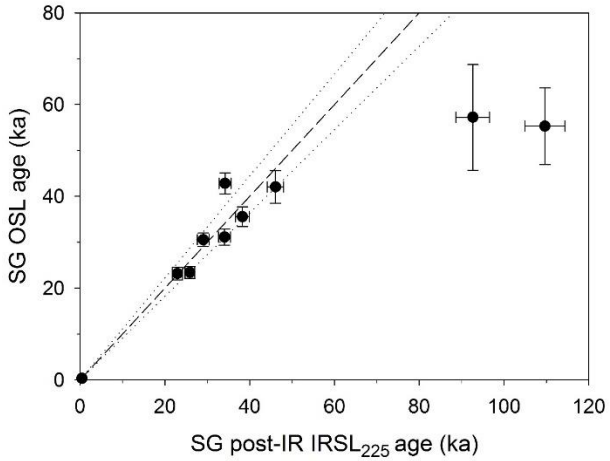

Figure 7: Comparison of the single grain (SG) quartz OSL ages and SG K-feldspar post-IR $IRSL_{225}$ ages. The dashed line shows the 1:1 relationship and the dotted lines ±10 %.

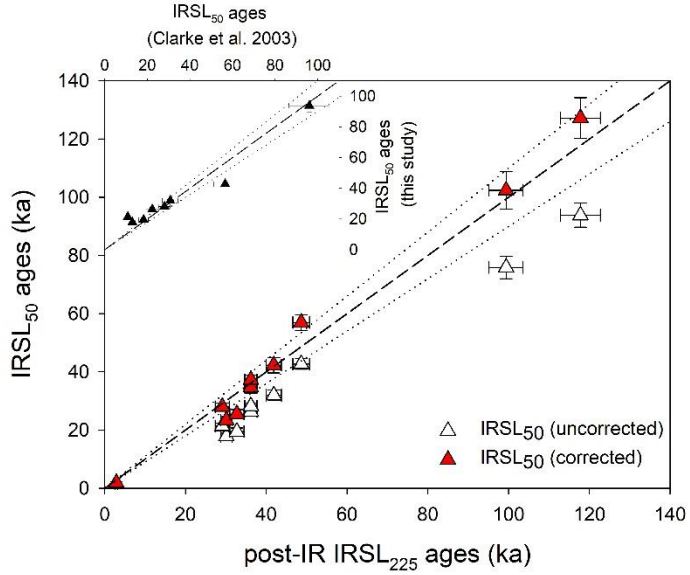

Figure 8: Comparison of the uncorrected post-IR $IRSL_{225}$ ages with the uncorrected (white triangles) and corrected (red triangles) $IRSL_{50}$ ages from this study. The $IRSL_{50}$ ages were corrected using the fading correction of Huntley and Lamothe (2001), with a g-value of 3.79 ± 0.20 %/decade and normalised to 2 days. Inset shows the uncorrected $IRSL_{50}$ ages from this study compared to the uncorrected $IRSL_{50}$ ages from Clarke et al. (2003).

Table 1: The existing radiocarbon chronology, published by Clarke et al. (2003). Radiocarbon ages have been recalibrated using the ShCal13 curve in OxCal v4.2 (Bronk Ramsey, 2009), and are presented in thousands of years (ka) from 2015 to facilitate comparison with the luminescence ages.

	Clarke et al. (2003) study			
Sample	C content (%)	C-14 age (years BP)	Calibrated age (ka)	Recalibrated age (ka)
Pta-5429	0.65	14500 ± 140	17.3	17.6 ± 0.4
Pta-6169	1.7	14260 ± 100	17.0	17.3 ± 0.3
Pta-6173	1.0	17100 ± 170	20.3	20.6 ± 0.5
Pta-5440	0.85	18700 ± 210	22.1	22.5 ± 0.5
Pta-6170	1.0	18600 ± 190	22.0	22.4 ± 0.5
Pta-5438	1.3	19800 ± 220	23.1	23.8 ± 0.5
Pta-6168	2.9	18700 ± 150	22.1	22.6 ± 0.4
Pta-5420	2.4	34500 ± 810	40.7	38.9 ± 2.0
Pta-5418	0.8	35700 ± 1000	42.3	40.3 ± 1.9
Pta-6411	1.0	31200 ± 700	36.8	35.3 ± 1.4
Pta-6413	1.0	37400 ± 1500	43.6	42.0 ± 2.9

Table 2: Sample dosimetry data, including uncorrected in-situ field and laboratory dosimetry measurements, and corrected environmental dose rates (Ḋ) for both quartz and K-feldspar.

Sample	Depth (m)	Direct measurements						Environmental dose rates	
		Field WC (%)	Saturated WC (%)	Field γ activity (Gy ka^{-1})[1]	Infinite matrix β activity (Gy ka^{-1})	α count rate (cts ks^{-1} cm^{-2})	Internal K content (wt%)	Quartz Ḋ (Gy ka^{-1})[2,4]	K-feldspar Ḋ (Gy ka^{-1})[3,4,5]
VRD09	0.3	1.9	41.4	1.146 ± 0.057	2.74 ± 0.09	0.562 ± 0.010	14.50 ± 1.15	2.86 ± 0.12	3.72 ± 0.14
VRD08	3.4	0.5	-	1.121 ± 0.056	2.40 ± 0.02	0.420 ± 0.008	14.25 ± 0.68	2.55 ± 0.10	3.37 ± 0.13
VRD07	4.1	1.7	-	1.084 ± 0.054	2.90 ± 0.14	0.448 ± 0.008	14.24 ± 0.46	2.84 ± 0.12	3.67 ± 0.14
VRD06	5.7	1.0	48.2	1.068 ± 0.054	2.41 ± 0.11	0.452 ± 0.008	11.15 ± 0.61	2.48 ± 0.10	3.31 ± 0.12
VRD05	7.3	1.3	-	1.276 ± 0.064	2.72 ± 0.11	0.500 ± 0.009	15.47 ± 0.24	2.82 ± 0.12	3.66 ± 0.14
VRD04	8.1	1.7	-	1.033 ± 0.052	2.47 ± 0.09	0.455 ± 0.008	14.57 ± 0.71	2.48 ± 0.10	3.30 ± 0.13
VRD03	8.7	0.9	-	1.064 ± 0.053	2.52 ± 0.13	0.430 ± 0.008	15.13 ± 1.13	2.52 ± 0.11	3.34 ± 0.13
VRD02	10.0	2.0	-	1.069 ± 0.054	2.09 ± 0.03	0.459 ± 0.008	10.66 ± 0.20	2.25 ± 0.09	3.07 ± 0.12
VRD01	12.0	3.2	44.8	1.154 ± 0.058	2.35 ± 0.09	0.540 ± 0.009	11.40 ± 0.60	2.48 ± 0.10	3.32 ± 0.13
VRD10	14.5	4.1	42.7	1.660 ± 0.083	3.19 ± 0.12	0.849 ± 0.013	10.11 ± 0.44	3.41 ± 0.14	4.33 ± 0.17

[1]Measured value was corrected for the modern field water content prior to dosimetry calculations.
[2]Comprised of the external β dose rate, external γ dose rate and cosmic dose rate.
[3]Comprised of the external α dose rate, external β dose rate, external γ dose rate and cosmic dose rate. Also includes an internal β dose rate (0.70 ± 0.06 Gy ka^{-1}) calculated from assumed K content of 12.5 ± 0.5 % (Huntley and Baril 1997) and a K/Rb ratio of 200:1 (Mejdahl 1987).
[4]External beta and gamma dose rates were corrected for grain size attenuation and a burial water content of 30 ± 5 %.
[5]External alpha dose rate was corrected for grain size attenuation, water content and alpha attenuation.

Table 3: Protocols used to measure the (a) multiple grain (MG) and (b) single grain (SG) quartz OSL signal, and the (c) single grain (SG) K-feldspar post-IR $IRSL_{225}$ signal.

(a) MG Quartz OSL protocol

Step	Treatment	Measured
1	Dose	
2	Preheat at 220 °C for 10 s	
3	OSL at 125 °C for 40 s (LEDs)	L_x
4	Test dose (5 Gy)	
5	Preheat at 160 °C for 10 s	
6	OSL at 125 °C for 40 s (LEDs)	T_x
7	Return to step 1	

(b) SG Quartz OSL protocol

Step	Treatment	Measured
1	Dose	
2	Preheat at 220 °C for 10 s	
3	OSL at 125 °C for 1 s (Laser)	L_x
4	Test dose (5 Gy)	
5	Preheat at 160 °C for 10 s	
6	OSL at 125 °C for 1 s (Laser)	T_x
7	Return to step 1	

(c) SG K-feldspar post-IR IRSL protocol

Step	Treatment	Measured
1	Dose	
2	Preheat at 250 °C for 60 s	
3	IRSL at 50 °C for 200 s (LEDs)	
4	IRSL at 225 °C for 2 s (Laser)	L_x
5	Test dose (30% of average D_e)	
6	Preheat at 250 °C for 60 s	
7	IRSL at 50 °C for 200 s (LEDs)	
8	IRSL at 225 °C for 2 s (Laser)	T_x
9	IRSL at 290 °C for 100 s (LEDs)	
10	Return to step 1	

Table 4: Results of the single grain dose recovery tests using quartz OSL and K-feldspar post-IR $IRSL_{225}$, including the given dose (GD), measured/given dose ratio (M/G ratio), total number of grains measured (N), number of grains in the dose distribution (n), number of saturated grains (n_{sat}) and overdispersion (OD).

Sample	Mineral	Protocol	GD (Gy)	M/G ratio	N	n	n_{sat}	OD (%)
Aber215/VRD09	Qtz	SG	5	1.05 ± 0.03	300	36	0	11
	Kf	SG	5	1.02 ± 0.01	300	226	0	6
Aber215/VRD06	Qtz	MG	91	0.93 ± 0.05	3	3	0	0
	Qtz	SG	90	0.91 ± 0.03	500	61	22	9
	Kf	SG	100	0.99 ± 0.01	300	228	0	7
Aber215/VRD01	Qtz	MG	182	0.88 ± 0.07	3	3	0	0
	Qtz	SG	150	0.79 ± 0.04	500	21	41	0
	Kf	SG	300	0.94 ± 0.01	300	198	0	15

Table 5: Comparison of multiple grain (MG) quartz OSL, single grain (SG) quartz OSL, and SG feldspar post-IR IRSL data, including the total number of grains measured (N), the number of saturated grains (n_{sat}), the number of grains in the D_e distribution (n), the overdispersion (OD), the mean characteristic saturation dose (D_0) of the individual DRCs, the equivalent dose (D_e) and the age. Percentage values for n_{sat} and n refer to the proportion of accepted grains/aliquots in saturation or in the dose distribution, respectively.

Sample	Mineral	Protocol	Grain size (µm)	N	n_{sat}		n		OD (%)	D_0 (Gy)	D_e (Gy)[1]	Age (ka)
VRD09	Qtz	MG	180-212	24	0	(0%)	24	(100%)	75	40 ± 2	1.84 ± 0.14	0.64 ± 0.06
	Qtz	SG	180-212	1000	4	(4%)	92	(96%)	110	33 ± 2	0.93 ± 0.07	0.32 ± 0.03
	Kf	SG	180-212	500	0	(0%)	365	(100%)	101	98 ± 1	1.60 ± 0.08	0.43 ± 0.03
VRD08	Qtz	MG	180-212	24	2	(9%)	21	(91%)	26	37 ± 2	68.6 ± 4.2	26.9 ± 2.0
	Qtz	SG	180-212	1100	20	(20%)	82	(80%)	31	52 ± 4	59.6 ± 2.2	23.4 ± 1.3
	Kf	SG	180-212	800	10	(2%)	499	(98%)	49	200 ± 3	87.1 ± 1.9	25.9 ± 1.1
VRD07	Qtz	MG	180-212	20	2	(11%)	17	(89%)	18	43 ± 3	77.8 ± 3.9	27.4 ± 1.8
	Qtz	SG	180-212	1000	17	(18%)	78	(82%)	34	60 ± 3	65.7 ± 2.8	23.2 ± 1.4
	Kf	SG	180-212	600	8	(3%)	298	(97%)	63	205 ± 5	84.1 ± 3.1	22.9 ± 1.2
VRD06	Qtz	MG	150-180	24	2	(9%)	21	(91%)	15	55 ± 3	83.3 ± 3.1	33.6 ± 1.8
	Qtz	SG	150-180	1000	35	(23%)	115	(77%)	23	57 ± 2	75.8 ± 2.0	30.5 ± 1.5
	Kf	SG	180-212	700	0	(0%)	226	(100%)	45	246 ± 5	96.2 ± 2.9	29.0 ± 1.4
VRD05	Qtz	MG	180-212	24	10	(43%)	13	(57%)	10	45 ± 2	101 ± 4	35.9 ± 2.1
	Qtz	SG	180-212	1400	62	(41%)	89	(59%)	30	58 ± 2	87.8 ± 3.3	31.1 ± 1.7
	Kf	SG	180-212	600	1	(0%)	380	(100%)	33	249 ± 3	125 ± 2	34.1 ± 1.4
VRD04	Qtz	MG	150-180	24	7	(32%)	15	(68%)	23	56 ± 4	140 ± 10	56.6 ± 4.6
	Qtz	SG	150-180	1200	69	(43%)	90	(57%)	24	63 ± 2	106 ± 3	42.8 ± 2.3
	Kf	SG	150-180	700	1	(0%)	356	(100%)	31	238 ± 3	113 ± 2	34.2 ± 1.4
VRD03	Qtz	MG	180-212	24	11	(52%)	10	(48%)	10	52 ± 3	121 ± 6	48.1 ± 3.0
	Qtz	SG	180-212	2000	132	(59%)	92	(41%)	35	50 ± 2	89.4 ± 3.8	35.6 ± 2.1
	Kf	SG	180-212	600	7	(2%)	357	(98%)	39	242 ± 4	128 ± 3	38.3 ± 1.7
VRD02	Qtz	MG	150-180	12	5	(42%)	7	(58%)	18	60 ± 7	155 ± 14	69.0 ± 6.9
	Qtz	SG	150-180	600	47	(60%)	31	(40%)	36	51 ± 3	94.4 ± 7.0	42.1 ± 3.6
	Kf	SG	180-212	500	0	(0%)	294	(100%)	28	287 ± 6	141 ± 2	46.1 ± 1.9
VRD01	Qtz	MG	180-212	12	10	(83%)	2	(17%)	8	54 ± 10	150 ± 14	60.5 ± 6.3

	Qtz	SG	180-212	400	56	(92%)	5	(8%)	12	45 ± 2	137 ± 20	55.3 ± 8.4
	Kf	SG	150-180	500	3	(1%)	362	(99%)	37	353 ± 6	364 ± 7	109 ± 4
VRD10	Qtz	MG	150-180	15	12	(86%)	2	(14%)	23	63 ± 11	180 ± 32	52.8 ± 9.7
	Qtz	SG	150-180	500	28	(85%)	5	(15%)	34	62 ± 4	195 ± 38	57.2 ± 11.5
	Kf	SG	150-180	500	8	(2%)	365	(98%)	34	377 ± 7	401 ± 7	92.6 ± 4.0

[1]The Central Age Model (CAM) was used to determine the D_e value for all samples, except Aber215/VRD09 for which the unlogged 3-component MAM (Arnold et al 2009) was used in order to include negative D_e values in the calculation. A sigma_b value of 0.15 and 0.20 was used in the MAM calculation for MG and SG respectively (see text for details). For the quartz MG dose distributions where n=2 (Aber215/VRD01 and Aber215/VRD10) the mean D_e is shown.

Table 6: Summary of single grain quartz OSL and K-feldspar post-IR $IRSL_{225}$ measurements and acceptance criteria

Sample	VRD09	VRD08	VRD07	VRD06	VRD05	VRD04	VRD03	VRD02	VRD01	VRD10
QUARTZ OSL										
Total grains measured	1000	1100	1000	1000	1400	1200	2000	600	400	500
Signal indistinguishable from BG level	716	827	745	627	1005	782	1520	363	253	379
Grains producing a dose response curve	284	273	255	373	395	418	480	237	147	121
Number of saturated grains	4	20	17	35	62	69	132	47	56	28
Grains that failed acceptance criteria:	**187**	**171**	**160**	**223**	**244**	**259**	**255**	**159**	**86**	**88**
Recycling	92	102	92	139	138	159	155	117	59	53
Recuperation	45	11	12	13	16	11	11	5	4	6
Maximum test dose error	50	58	56	71	90	89	89	37	23	29
Grains in D_e distribution	**93**	**82**	**78**	**115**	**89**	**90**	**93**	**31**	**5**	**5**
K-FELDSPAR POST-IR IRSL										
Total grains measured	500	800	600	700	600	700	600	500	500	500
Signal indistinguishable from BG level	71	5	61	21	5	42	36	16	36	4
Grains producing a dose response curve	429	795	539	679	595	658	564	484	464	496
Number of saturated grains	0	10	8	0	1	1	7	0	3	8
Grains that failed acceptance criteria:	**64**	**286**	**233**	**453**	**214**	**301**	**200**	**190**	**99**	**123**
Recycling	52	148	122	198	128	162	107	132	91	112
Recuperation	10	138	87	217	80	119	81	35	0	1
Maximum test dose error	2	0	24	38	6	20	12	23	8	10
Grains in D_e distribution	**365**	**499**	**298**	**226**	**380**	**356**	**357**	**294**	**362**	**365**